ACS OMEGA

http://pubs.acs.org/journal/acsodf

Article

Mechanism Investigations on Water Gas Shift Reaction over Cu(111), Cu(100), and Cu(211) Surfaces

Zhiyuan Li,* Na Li, Nan Wang, Bing Zhou, Pan Yin, Boyu Song, Jun Yu, and Yusen Yang

Cite This: *ACS Omega* 2022, 7, 3514−3521

Read Online

ACCESS | Metrics & More | Article Recommendations | Supporting Information

ABSTRACT: Cu-based catalysts are commonly applied in low-temperature water gas shift (WGS) reactions, owing to their low cost and high catalytic activity. The influence of different Cu surfaces on catalytic activity and mechanism over the WGS reaction remains unclear. In this work, the effect of different structures of surfaces on the WGS mechanism is studied using density functional theory (DFT). Three surface terminations (Cu(100), Cu(111), and Cu(211)) of Cu are considered, and the coordination number (CN) of the active Cu site is in the range from 7 to 9. The most stable surface is Cu(211). Then, d-band center values are calculated, which decrease in the following sequence: Cu(211) > Cu(100) > Cu(111). This shows that d-band center values decrease with increasing coordination number. The increase in the centers of the d-band leads to an increase in the adsorption strength of CO and H_2O adsorbates, which is in line with the theory of the d-band center. In addition, the further calculated mechanism for WGS reaction over three different Cu surfaces illustrates that the carboxyl path is the most favorable mechanism, and the rate-determining step is H_2O dissociation. Cu(211) shows excellent WGS catalytic performance, better than the Cu(100) and Cu(111) surfaces. This work provides theoretical insights into the rational design of highly active Cu-based catalysts toward WGS reaction.

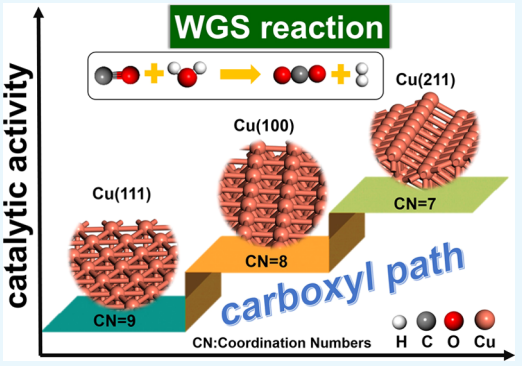

INTRODUCTION

In the field of heterogeneous catalysis, structural sensitivity is one of the significant issues in the understanding and analysis of active sites. It is challenging to determine the structural sensitivity of catalysts to obtain optimal and stable reaction activity.[1] There have been many reports on the nature of structural sensitivity using different preparation methods, structural characterization, surface studies, and density functional theory (DFT) calculations.[2−4] However, due to the lack of understanding of the reaction mechanism and kinetic information, there are still speculations about why and how structural sensitivity occurs at the atomic level. The theoretical analysis of surface reaction, geometric structure, and electronic structure is highly critical and necessary, which can provide key information for discovering and understanding the structure-sensitive characteristics presented on the various surfaces.

The water gas shift (WGS) reaction is a significant industrial reaction used to produce high-purity H_2,[5−8] which catalytic on the Cu catalysts are considered to be a representative structure-sensitive reaction.[9,10] The structure sensitivity has been explored and studied using theoretical methods, but the reason why WGS reaction is sensitive to structure is still unclear.[11,12] The WGS reaction mechanisms have been well-studied, which have a "redox path", "carboxyl intermediate path", and a "formate intermediate path".[13−16] Chutia et al. reported that on the Pd(100) surface, the WGS reaction proceeds simultaneously through direct oxidation and the COOH intermediate pathways.[17] Mohsenzadeh et al. studied the WGS reaction on Ni(100), Ni(110), and Ni(111) using DFT methods.[18] Cao et al. studied the structure dependence of H_2 adsorption and desorption on Cu(211) and flat Cu(111) and found that H_2 is more easily dissociates and desorbs on the flat surface.[19] However, the influences of different Cu surfaces on the mechanism, catalytic activity, and structure sensitivity toward the WGS reaction are still not clear.

In our work, a theoretical study toward WGS reaction on Cu(100), Cu(111), and Cu(211) catalysts is carried out (Figure 1). The carboxyl path is the dominant pathway over Cu(100), Cu(111), and Cu(211), and the rate-determining steps are the H_2O* dissociation steps. Cu(211) presents the lowest activation energies for the reaction elementary steps, and it is considered to be the most active surface, and Cu(111) is the worst. This study provides useful theoretical information for the WGS reaction mechanism on the Cu catalyst surfaces and is beneficial to the design of highly stable and effective Cu-based catalysts.

Received: October 26, 2021
Accepted: January 5, 2022
Published: January 14, 2022

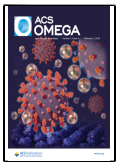

https://doi.org/10.1021/acsomega.1c05991
ACS Omega 2022, 7, 3514−3521

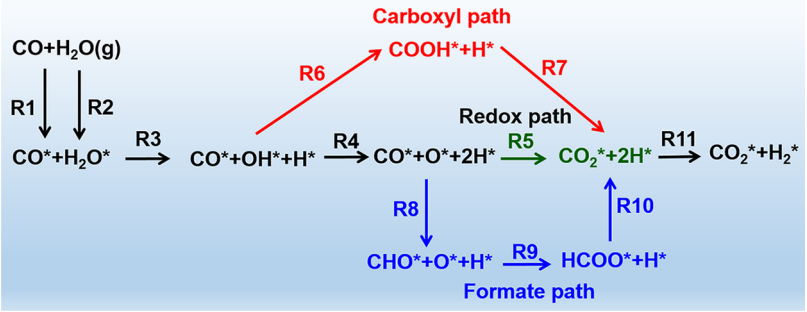

Figure 1. WGS reaction paths.

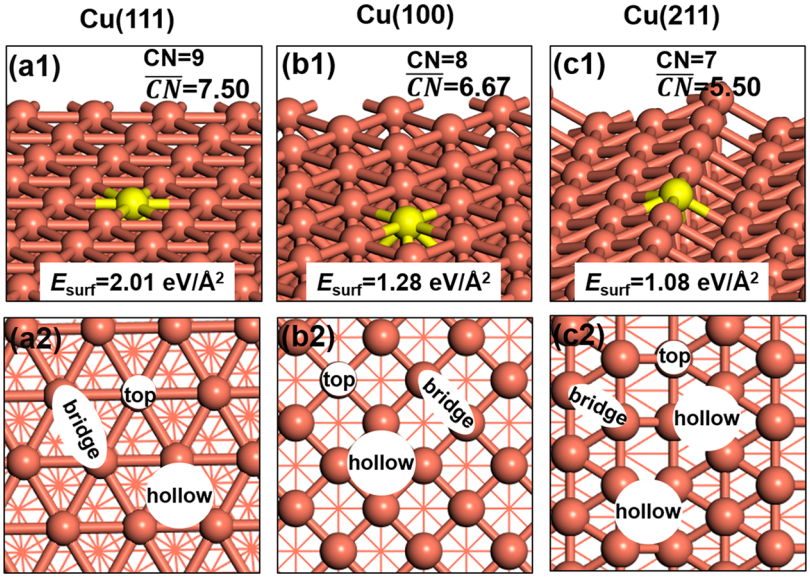

Figure 2. Top view of optimized structures and the schematic of adsorption sites of (a) Cu (111), (b) Cu (100), and (c) Cu (211) surfaces (Cu: brown).

Table 1. Adsorption Energies (E_{ads}, in eV) and Bond Distance (d, in Å) between Species and Surface Atoms Involved in the WGS Reaction on Cu(111), Cu(100), and Cu(211) Surfaces

species	H_2O	CO	OH	H	H_2	CO_2	
Cu(111)	site	top	hollow	hollow	hollow	bridge	top
	E_{ads}	−0.20	−0.97	−3.25	−0.29	−0.02	−0.04
	d	2.35	2.04/2.04/2.04	2.02/2.02/2.03	1.73/1.73/1.73	3.24/3.02	3.67
Cu(100)	site	top	hollow	hollow	hollow	top	bridge
	E_{ads}	−0.24	−1.04	−3.28	−0.31	−0.02	−0.05
	d	2.28	2.14/2.14/2.15	2.11/2.19/2.17	1.88	3.66	4.05/4.10
Cu(211)	site	top	hollow	bridge	hollow	hollow	top
	E_{ads}	−0.36	−0.89	−3.52	−0.25	−0.01	−0.05
	d	2.22	2.00/2.00/2.15	1.95/1.95	1.72/1.72/1.81	3.37	4.27

RESULTS AND DISCUSSION

Geometries and Adsorption Sites on Cu(111), Cu(100), and Cu(211) Surfaces. Three models with various surfaces are established to obtain surface active sites (Cu(111), Cu(100), and Cu(211)). The active sites with a coordination number (CN) of 7−9 for metallic Cu have been selected. The site with CN = 7 represents the step site, and the terrace sites are the sites corresponding to the coordination number CN = 8/9. In surface chemistry, chemical properties can be better described by the generalized coordination number ($\overline{CN}$) than CN.[20,21] As shown in Figure 2a1−c1, the surface energies of the three systems can reflect the stabilities of their surfaces. The lower the surface energy, the more stable the catalyst surface. Cu(111) presents the highest CN (9) and surface energy (E_{surf} = 2.01 eV/Å^2), followed by Cu(100) (E_{surf} = 1.28 eV/Å^2), and the lowest surface energy is presented by the Cu (211) surface (E_{surf} = 1.08 eV/Å^2). The surface energy increases by degrees with increasing coordination number (CN), CN = 7−9.

The possible adsorption sites of Cu(111), Cu(100), and Cu(211) surfaces are displayed in Figure 2a2−c2. There are highly symmetrical adsorption sites on these surfaces, which are top, bridge, three-fold hollow, and four-fold hollow sites. The adsorption and activation of reactant, intermediate, or

https://doi.org/10.1021/acsomega.1c05991
ACS Omega 2022, 7, 3514−3521

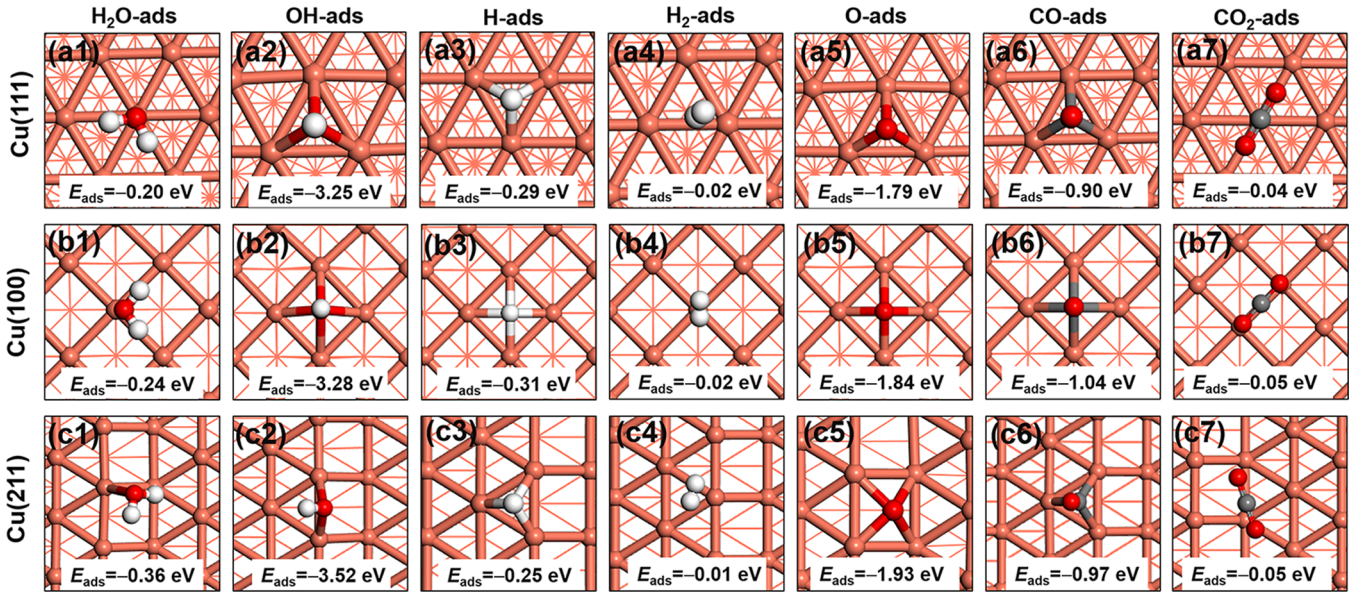

Figure 3. Top view of the optimized adsorption structures of H_2O, CO, OH, H, O, H_2, and CO_2 on (a) Cu (111), (b) Cu (100), and (c) Cu (211) surfaces, along with the adsorption energies (E_{ads}) (Cu: brown).

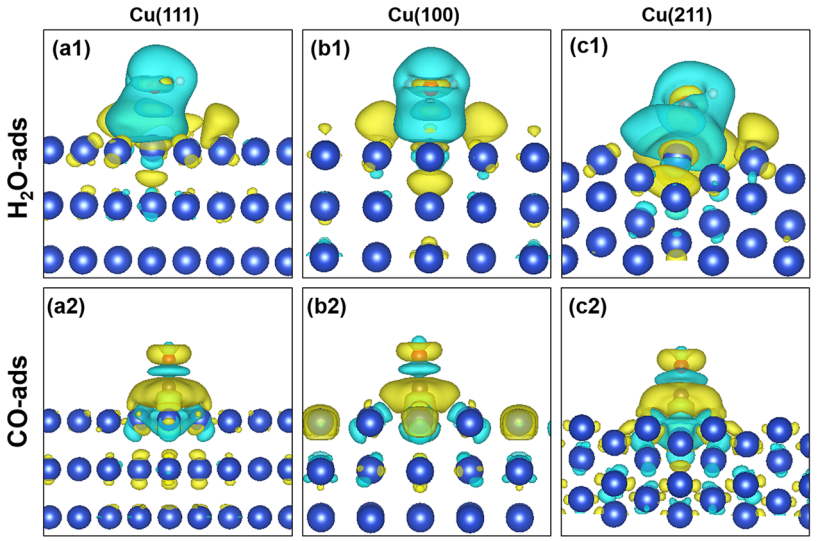

Figure 4. Electron density difference diagrams of H_2O and CO adsorption on (a) Cu(111), (b) Cu(100), and (c) Cu(211) surfaces. Blue represents an electron-loss region and yellow represents an electron-accumulation region.

product involved in WGS reaction on Cu(111), Cu(100), and Cu(211) consider these sites.

Adsorption Configurations and Energies of H_2O, CO, H_2, and CO_2 and Their Decomposition Intermediates (OH, O, and H) on Cu(111), Cu(100), and Cu(211) Surfaces. Geometry optimizations are performed for all adsorption sites, and then the structures of the corresponding species with the lowest energy are selected to study the reaction mechanism (Figures S1−S3). Table 1 and Figure 3 show the lowest energy structures of reactive species in the WGS reaction.

For Cu(111), Cu(100), and Cu(211), H_2O is weakly bound to the Cu atom site, with adsorption energies of −0.20, −0.24, and −0.36 eV, respectively, which are close to the values reported in the literature (Table S1). The Cu(211) surface has the strongest adsorption of H_2O. OH binds preferentially on hollow sites on both (111) (E_{ads}(OH) = −3.25 eV) and (100) (E_{ads}(OH) = −3.28 eV) surfaces and is adsorbed at the bridge site on Cu(211) (E_{ads}(OH) = −3.52 eV). Whereas H_2O and OH are most stable on Cu(211). O adsorbs stably on hollow sites on Cu(100), Cu(111), and Cu(211). H species binds the hollow sites on Cu(111), (100), and (211) with similar adsorption energies, −0.29, −0.31, and −0.25 eV, respectively.

CO is adsorbed stably at the hollow site, hollow site, and hollow site on Cu(111) (E_{ads}(CO) = −0.90 eV), Cu(100) (E_{ads}(CO) = −1.04 eV), and Cu(211) (E_{ads}(CO) = −0.97 eV) surfaces, respectively. H_2 produces molecular adsorption configuration at the bridge site, top site, and hollow site on Cu(111) (E_{ads}(H_2) = −0.02 eV), Cu(100) (E_{ads}(H_2) = −0.02 eV), and Cu(211) (E_{ads}(H_2) = −0.01 eV) surfaces, respectively. H_2 adsorption is the weakest on the Cu(211) surface. CO_2 species are quite weakly adsorbed *via* van der Waals interaction due to their saturated nature. CO_2 adsorption energies decrease in the following order: Cu(211)

https://doi.org/10.1021/acsomega.1c05991
ACS Omega 2022, 7, 3514−3521

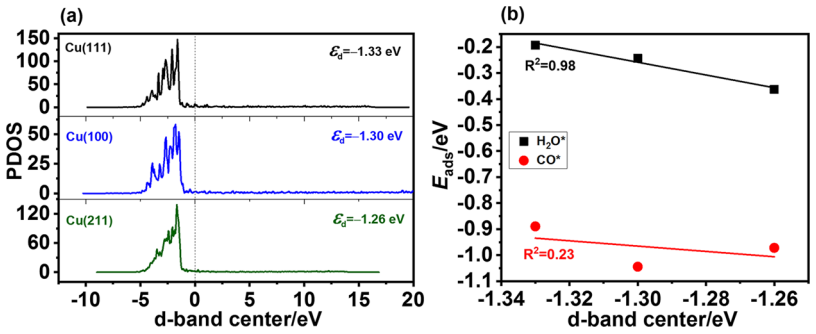

Figure 5. d-Band center values of Cu(111), Cu(100), and Cu(211) surfaces (a) and the fitting curve of the d-band center vs the adsorption energies (E_{ads}) of H_2O*and CO* on these surfaces (b).

~ Cu(100)> Cu(111). The low adsorption of H_2 and CO_2 on these surfaces shows that once the H_2 and CO_2 products are formed, they are easily desorbed from the surfaces.

Figure 4a1−c1 shows the difference in electron density of H_2O adsorption. All three surfaces ((111), (100), (211)) reflect a net electron flow from surface Cu atoms (yellow area) to H_2O molecules (blue area) after H_2O is adsorbed. As the coordination number decreases, the electron accumulation and overlap area around Cu atoms gradually increase, which reveals that the interaction between H_2O and Cu sites increases. Therefore, the increasing order of adsorption energy is Cu(211) > Cu(100) > Cu(111). Cu(211) is the most advantageous for H_2O adsorption. For the CO adsorption process (Figure 4a2−c2), the net electron flow from the Cu atom site to the CO molecule is displayed on these three surfaces. The accumulation of electrons near Cu sites gradually decreases, and the order is Cu(100) > Cu(211) > Cu(111).

d-Band Center Energy vs Adsorption Energy. The interaction between the valence state of adsorbates and the surface metal d-band can be predicted by the d-band central energy.[22] The d-band center energy values of Cu(111), Cu(100), and Cu(211) are obtained (Figure 5a). The d-band centers calculated on the three surfaces reduce in the order Cu(211) (ε_d = −1.26 eV) > Cu(100) (ε_d = −1.30 eV) > Cu(111) (ε_d = −1.33 eV). This shows that the center value of the d-band decreases with an increase of the coordination number.

As shown in Figure 5b, the fitting curves of the d-band center and adsorption energies of H_2O and CO on Cu(111), Cu(100), and Cu(211) are obtained. The increase of the d-band center results in an improvement in adsorption energies of H_2O*, which is in accordance with the theory of the d-band center. The factors affecting adsorption energies are of two types: geometric and electron factors.[23] CO is adsorbed stably at the three-hollow site, four-hollow site, and the three-hollow site on Cu(111), Cu(100), and Cu(211), respectively. The d-band center value only describes the changes of the surface electronic structure. The different geometric sites may lead to different adsorption energies.

WGS Reaction Mechanism over Cu(111), Cu(100), and Cu(211) Surfaces. DFT theoretical calculations are carried out according to the WGS reaction mechanism (redox paths, carboxyl (COOH) paths, and formate (HCOO) paths) shown in Figure 1.

R3: $H_2O^* + * \rightleftharpoons OH^* + H^*$

The WGS reaction starts with the partial dissociation of H_2O. The activation energy barriers (E_a) of H_2O dissociation steps are 1.31, 1.19, and 0.94 eV on Cu(111), Cu(100), and Cu(211), respectively (Figure 6). The dissociation barriers of

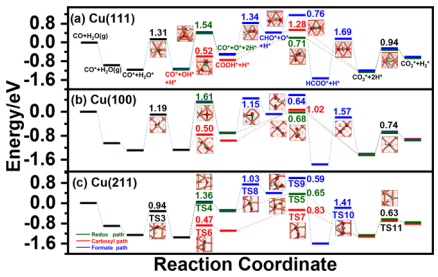

Figure 6. Energy profiles of three WGS reaction paths on the (a) Cu(111), (b) Cu(100), and (c) Cu(211) surfaces. The numbers (in eV) are energy barrier values of the corresponding steps. The vignette is the transition-state (TS) structures of the corresponding elementary steps on these surfaces (H, white; O, red; C, dark gray; Cu, brown).

these three surfaces are quite different, indicating that the WGS reaction is the reaction of structure sensitivity. Wang et al. reported that the energy barriers for the H_2O dissociation decrease in the sequence of Cu(111) > Cu(100) > Cu(110), which is consistent with our calculation; Cu(111) shows the highest activation energy barrier of the H_2O dissociation step.[2] As the coordination number decreases, the ease of H_2O dissociation increases, which is in accordance with the abovementioned results. Cu(211) is most conducive to H_2O dissociation.

R4: $OH^* + * \rightleftharpoons H^* + O^*$

The OH* dissociation step is the atomic O source for both the redox and formate paths. The hollow sites are the most stable sites for OH, H, and O species adsorption (Table 1) on Cu(111). The OH* species dissociates on Cu(100) *via* the transition state, with O near the hollow site and H located at the bridge site. On Cu(211), OH binds preferentially on the bridge site, and O species adsorbs at the hollow site. R4 has the lowest activation energy (1.36 eV) on Cu(211), compared to Cu(111) (1.54 eV) and Cu(100) (1.61 eV) surfaces.

Redox Path.

R5: $CO^* + O^* \rightleftharpoons CO_2^* + *$

For the Cu(111) surface, CO* adsorbs at the hollow site (E_{ads} = −0.90 eV) in the initial state, and O* shifts from the hollow site close to CO*. The distance between CO* and O* at the transition state (TS5) is 2.16, 1.62, and 1.79 Å on Cu(111), Cu(100), and Cu(211), respectively (Figures S4−S6). The energy barriers of R5 are 0.71, 0.68, and 0.65 eV on

https://doi.org/10.1021/acsomega.1c05991
ACS Omega 2022, 7, 3514−3521

Cu(111), Cu(100), and Cu(211), respectively, which reveals that the kinetics of the CO oxidation process on Cu(211) is most favorable. CO_2 adsorption energies on Cu(111), Cu(100), and Cu(211) are −0.04, −0.05, and −0.05 eV, respectively. This suggests that CO_2 is easily desorbed, once formed.

Carboxyl Path.

R6: CO* + OH* ⇌ COOH* and R7: COOH* ⇌ CO_2* + H*

Co-adsorbed CO* and OH* form a carboxyl (COOH*) intermediate, and the COOH* intermediate is directly decomposed into co-adsorbed CO_2 and H through O−H bond cleavage. As shown in Figure 6, the carboxyl formation steps (R6) are all endothermic on Cu(111), Cu(100), and Cu(211) (Table S2) with barriers of 0.52, 0.50, and 0.47 eV, respectively. At the transition state (TS6), the distances between CO* and OH* are 1.76, 1.89, and 1.71 Å, respectively (Figures S4−S6, respectively). The reaction energy and the energy barrier are different, which is owing to the relative stability of CO and OH on the surfaces of the three systems. For R7, at the transition state (TS7), the H(COOH)−O distances are 1.98, 1.80, and 1.99 Å, respectively (Figures S4−S6, respectively). COOH dehydrogenation is exothermic by −0.57, −0.38, and −0.21 eV, respectively (Table S2). The energy barrier order of the R7 dissociation step on the different surfaces is Cu(111) (E_a = 1.28 eV) > Cu(100) (E_a = 1.02 eV) > Cu(211) (E_a = 0.83 eV). R6 and R7 steps are the most feasible on the Cu(211) surface due to both steps presenting the lowest energy barriers on the three surfaces.

Formate Path.

R8: CO* + H* ⇌ CHO*, R9: CHO* + O* ⇌ HCOO* and R10: HCOO* ⇌ CO_2* + H*

The adsorption energies of CHO* are −1.48 eV (bridge site), −1.58 eV (hollow site), and −1.50 eV (hollow site) on Cu(111), Cu(100), and Cu(211), respectively. HCOO* is adsorbed at the bridge site with −2.90, −2.97, and −3.27 eV on Cu(111), Cu(100), and Cu(211), respectively. The order of surfaces in activation energy (TS8) of R8 is Cu(111) (E_a = 1.34 eV) > Cu(100) (E_a = 1.15 eV) > Cu(211) (E_a = 1.03 eV). The activation energies (TS9) of R9 are 0.76, 0.64, and 0.59 eV, respectively. For R10, the energy barrier (E_a) of HCOO dehydrogenation increases in the sequence Cu(211) < Cu(100) < Cu(111) (1.41, 1.57, and 1.69 eV, respectively). On the three Cu surfaces, R10 exhibits a higher activation energy barrier than R8 or R9. Therefore, R10 is the most difficult process in this path. The formate intermediate only acts as a "spectator" species. R10 presents the highest energy barrier; thus, on comparing the redox and the carboxyl paths, it is most difficult for the formate path to occur.

R11: H* + H* → H_2* + *

The adsorption energies of H_2 on Cu(111), Cu(100), and Cu(211) are very weak. This reveals that once H_2 is formed, it is likely to be immediately desorbed from these surfaces. The activation energy barriers (TS11) of forming H_2 (R11) are 0.94, 0.74, and 0.63 eV on Cu(111), Cu(100), and Cu(211), respectively (Figure 6), which indicates that it is easiest for the Cu(211) surface to form H_2.

Summarily, the energy barriers of the carboxyl path are lower than all of those of the redox or formate path, indicating that the carboxyl path is the dominant pathway over Cu(111), Cu(100), and Cu(211), and the rate-determining steps correspond to the dissociation of H_2O* (R3). Cu(211) exhibits the lowest activation energy barrier of the WGS reaction steps. Compared with the terrace Cu(111) surface, the step sites reduce the energy barriers of rate-determining steps. This is consistent with our calculation results and further verifies that the step sites play a critical role in improving the WGS reaction activity.

As shown in Figure 7, the TOFs are obtained using eq 6 (Table S3), and the E_a^{eff} value is calculated based on the WGS energy profile (Figure S7). As the temperature increases (from 423 to 723 K), the log(TOFs) increases from −2.31 to 4.26, 0.79 to 6.07, and 3.06 to 7.39 s^{-1} on Cu(111), Cu(100), and Cu(211), respectively. This shows that the reaction activity increases with the enhancement of temperature. At the same temperature, the TOF values of different Cu surfaces (Cu(211) > Cu(100) > Cu(111)) present a downward trend, and the maximum TOF is obtained on Cu(211), which reveals that Cu(211) exhibits the highest catalytic activity, followed by Cu(100) and Cu(111) surfaces.

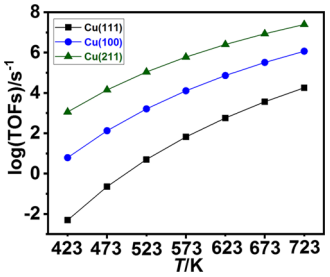

Figure 7. TOFs (s^{-1}) of WGS reaction as a function of temperature (423−723 K).

CONCLUSIONS

The DFT investigations for WGS reaction on three surface terminations of Cu with various coordination numbers were carried out. With decreasing CN, the surface energy gradually decreases, and the Cu(211) surface is the most stable surface. The increase of the d-band center results in enhancement of the adsorption strength of H_2O* and CO* adsorbates. Moreover, the WGS reaction mechanism reveals that on comparing Cu(111) and Cu(100), Cu(211) exhibits the lowest activation energy barrier of reaction steps and is most conducive to WGS reaction. The carboxyl path is the dominant path, and the rate-determining steps correspond to H_2O* dissociation. This work offers a theoretical understanding of the study of Cu-based catalysts and helps to rationally design high-activity catalysts for WGS reaction.

COMPUTATIONAL DETAILS

Reaction Paths. There are three probable reaction pathways for WGS (Figure 1).[15,16] The catalyst surfaces first adsorb CO (R1) and H_2O (R2), followed by partial (R3) and complete (R4) dissociation of H_2O. For the redox path, CO is oxidized by O to CO_2 (R5). For the carboxyl path, CO and OH combine to form the COOH intermediate (R6) and further produce CO_2 by COOH dehydrogenation (R7). CO is oxidized by H to CHO (R8), and CHO is oxidized with O to

https://doi.org/10.1021/acsomega.1c05991
ACS Omega 2022, 7, 3514−3521

HCOO intermediates (R9) and further forms CO_2 by HCOO dissociation (R10) in the formate path. H_2 is formed by the binding of two H* (R11). The elementary reaction steps involved in WGS will be studied.

Computational Models. In this work, a Cu catalyst is built (Cu-PDF#04-0836). The lattice constant optimized for the Cu system is $a = b = c = 3.64$ Å, $\alpha = \beta = \gamma = 90°$ (Figure S8). Cu(100), Cu(111), and Cu(211) are cleaved from optimized bulk Cu (Figure 2). Three-layer slabs with $p(2 \times 2)$ supercells are cleaved. The vacuum thickness is set to 15 Å (Figure S9). The bottom layer of atoms is constrained while the upper layers are allowed to relax.

Theoretical Methods. In this study, the calculations are based on DFT and performed using the Vienna ab-initio simulation package (VASP).[24−26] The electronic exchange and correlation components are described by the Perdew−Burke−Ernzerhof (PBE) function of generalized gradient approximation (GGA).[27] The basis test set in different computational methods proves that the PBE method is most reasonable (Figures S10−S11, Tables S4−S6). The interaction between valence electrons and ion cores is described by the projector augmented wave (PAW) method.[28,29] The cutoff energy is set as 500 eV and the convergence criterion of force threshold on each atom relaxed below 0.05 eV/Å is performed. The *k*-point is set as 5 × 5 × 1 to determine system geometries and energies. Transition states (TSs) are located with the CI-NEB method.[30,31]

The adsorption energies (E_{ads}) are obtained by the energy difference between the optimized surface including the adsorbed species (E_{total}) and the optimized clean surface with molecules in the gas phase ($E_g + E_{slab}$).

$$E_{ads} = E_{total} - (E_g + E_{slab}) \tag{1}$$

The energy barrier (E_a) is calculated by the energy difference between the transition state (E_{TS}) and the initial state (E_{IS}), which is defined by

$$E_a = E_{TS} - E_{IS} \tag{2}$$

Surface active sites are described by generalized coordination numbers (CN),[32] and the generalized coordination number of atom i is defined as

$$\overline{CN}(i) = \sum_{i=1}^{nj} cn(j) n_j / cn_{max} \tag{3}$$

Here, atom j is the neighbor of the atom i, n_j represents the usual coordination number of j, and cn_{max} refers to the maximum coordination number for the Cu bulk (fcc Cu crystal: $cn_{max} = 12$).

The surface energy (E_{surf}) is expressed as the energy required to cut an unlimited crystal into two parts, that is, the energy required to be a new surface. The calculation formula[33] is as follows

$$E_{surf} = \frac{1}{2A}(E_{slab} - E_{bulk}) \tag{4}$$

Here, E_{slab} refers to the slab total energy and E_{bulk} represents the bulk energy. It is generally believed that the surface with lower surface energy is easier to be formed.

The d-band center (ε_d) is usually obtained to predict the reactivity trend on different metal surfaces, and the d-band center occupied is obtained using the equation[34,35]

$$\varepsilon_d = \frac{\int_{-\infty}^{E_f} E\rho_d(E)dE}{\int_{-\infty}^{E_f} \rho(E)dE} \tag{5}$$

Here, ρ_d refers to the projected state density (PDOS) of the atom d-band of catalyst surfaces.

Based on the energy span theory, the turnover frequencies (TOFs) can be obtained to evaluate the catalytic activity.[36−38] The calculated formula can be defined by eq 6

$$TOF \approx \frac{k_B T}{h} e^{-E_a^{eff}/RT} \tag{6}$$

where k_B is the Boltzmann constant, which is 1.38×10^{-23} J/K; T is the operating temperature (423−723 K); h is the Planck constant, 6.63×10^{-34} J/s^{-1}; and E_a^{eff} refers to the effective barrier toward WGS reaction, which reflects the reaction activity. A lower effective barrier means a more catalytically active surface. E_a^{eff} is obtained by the energy difference between the transition state determined by TOF and the intermediate determined by TOF.

■ ASSOCIATED CONTENT

Supporting Information

The Supporting Information is available free of charge at https://pubs.acs.org/doi/10.1021/acsomega.1c05991.

Adsorption site test (Figures S1−S3, Table S1); WGS elementary reaction steps on Cu(111), Cu(100), and Cu(211) surfaces (Figures S4−S6, Table S2); determination of the effective barriers (Figure S7, Table S3); structural details of Cu (Figure S8); supercell convergence test of Cu(111), Cu(100), and Cu(211) surfaces (Figure S9); and computational method test (Figures S10 and S11, Tables S4−S6) (PDF)

■ AUTHOR INFORMATION

Corresponding Author

Zhiyuan Li − *Stated Grid Integrated Energy Service Group Co., Ltd., Beijing 100052, P. R. China*; Phone: +86-10-63505060; Email: sailorlzy@163.com; Fax: +86-10-63505555

Authors

Na Li − *Stated Grid Integrated Energy Service Group Co., Ltd., Beijing 100052, P. R. China*

Nan Wang − *Stated Grid Integrated Energy Service Group Co., Ltd., Beijing 100052, P. R. China*

Bing Zhou − *Stated Grid Integrated Energy Service Group Co., Ltd., Beijing 100052, P. R. China*

Pan Yin − *State Key Laboratory of Chemical Resource Engineering, Beijing Advanced Innovation Center for Soft Matter Science and Engineering, Beijing University of Chemical Technology, Beijing 100029, P. R. China*

Boyu Song − *State Key Laboratory of Chemical Resource Engineering, Beijing Advanced Innovation Center for Soft Matter Science and Engineering, Beijing University of Chemical Technology, Beijing 100029, P. R. China*

Jun Yu − *State Key Laboratory of Chemical Resource Engineering, Beijing Advanced Innovation Center for Soft Matter Science and Engineering, Beijing University of Chemical Technology, Beijing 100029, P. R. China*

Yusen Yang − *State Key Laboratory of Chemical Resource Engineering, Beijing Advanced Innovation Center for Soft*

https://doi.org/10.1021/acsomega.1c05991
ACS Omega 2022, 7, 3514−3521

Matter Science and Engineering, Beijing University of Chemical Technology, Beijing 100029, P. R. China

Complete contact information is available at: https://pubs.acs.org/10.1021/acsomega.1c05991

Notes

The authors declare no competing financial interest.

■ ACKNOWLEDGMENTS

This work was supported by the Science and Technology Project of Stated Grid Integrated Energy Service Group Co., Ltd.

■ REFERENCES

(1) Van Santen, R. A. Complementary Structure Sensitive and Insensitive Catalytic Relationships. *Acc. Chem. Res.* **2009**, *42*, 57−66.
(2) Wang, G. C.; Nakamura, J. Structure Sensitivity for Forward and Reverse Water-Gas Shift Reactions on Copper Surfaces: A DFT Study. *J. Phys. Chem. Lett.* **2010**, *1*, 3053−3057.
(3) Fajín, J. L. C.; Cordeiro, M. N. D. S.; Illas, F.; Gomes, J. R. B. Influence of Step Sites in the Molecular Mechanism of the Water Gas Shift Reaction Catalyzed by Copper. *J. Catal.* **2009**, *268*, 131−141.
(4) Tang, Q.; Chen, Z.; He, X. A Theoretical Study of the Water Gas Shift Reaction Mechanism on Cu(111) Model System. *Surf. Sci.* **2009**, *603*, 2138−2144.
(5) Zhang, X.; Zhang, M.; Deng, Y.; Xu, M.; Artiglia, L.; Wen, W.; Gao, R.; Chen, B.; Yao, S.; Zhang, X.; Peng, M.; Yan, J.; Li, A.; Jiang, Z.; Gao, X.; Cao, S.; Yang, C.; Kropf, A. J.; Shi, J.; Xie, J.; Bi, M.; van Bokhoven, J. A.; Li, Y. W.; Wen, X.; Flytzani-Stephanopoulos, M.; Shi, C.; Zhou, W.; Ma, D. A stable low-temperature H2-production catalyst by crowding Pt on α-MoC. *Nature* **2021**, *589*, 396−401.
(6) Xu, M.; Yao, S.; Rao, D.; Niu, Y.; Liu, N.; Peng, M.; Zhai, P.; Man, Y.; Zheng, L.; Wang, B.; Zhang, B.; Ma, D.; Wei, M. Insights into Interfacial Synergistic Catalysis over Ni@TiO_{2-x} Catalyst toward Water-Gas Shift Reaction. *J. Am. Chem. Soc.* **2018**, *140*, 11241−11251.
(7) Liu, N.; Xu, M.; Yang, Y.; Zhang, S.; Zhang, J.; Wang, W.; Zheng, L.; Hong, S.; Wei, M. $Au^{\delta-}$-O_v-Ti^{3+} Interfacial Site: Catalytic Active Center toward Low-Temperature Water Gas Shift Reaction. *ACS Catal.* **2019**, *9*, 2707−2717.
(8) Liu, N.; Yin, P.; Xu, M.; Yang, Y.; Zhang, S.; Zhang, J.; Meng, X.; Zhang, J.; Yu, J.; Man, Y.; Zhang, X.; Wei, M. The Catalytic Mechanism of the Au@TiO_{2-x}/ZnO Catalyst towards a Low-Temperature Water-Gas Shift Reaction. *Catal. Sci. Technol.* **2020**, *10*, 768−775.
(9) Nakamura, J.; Campbell, J. M.; Campbell, C. T. Kinetics and Mechanism of the Water-Gas Shift Reaction Catalysed by the Clean and Cs-Promoted Cu(110) Surface: A Comparison with Cu(111). *J. Chem. Soc. Faraday Trans.* **1990**, *86*, 2725−2734.
(10) Yoshihara, J.; Campbell, C. T. Methanol Synthesis and Reverse Water-Gas Shift Kinetics over Cu(110) Model Catalysts: Structural Sensitivity. *J. Catal.* **1996**, *161*, 776−782.
(11) Wang, G.; Jiang, L.; Cai, Z.; Pan, Y.; Zhao, X.; Huang, W.; Xie, K.; Li, Y.; Sun, Y.; Zhong, B. Surface Structure Sensitivity of the Water-Gas Shift Reaction on Cu(Hkl) Surfaces: A Theoretical Study. *J. Phys. Chem. B* **2003**, *107*, 557−562.
(12) Wang, G.; Jiang, L.; Pang, X.; Cai, Z.; Pan, Y.; Zhao, X.; Morikawa, Y.; Nakamura, J. A Theoretical Study of Surface-Structural Sensitivity of the Reverse Water-Gas Shift Reaction over Cu(Hkl) Surfaces. *Surf. Sci.* **2003**, *543*, 118−130.
(13) Gokhale, A. A.; Dumesic, J. A.; Mavrikakis, M. On the Mechanism of Low-Temperature Water Gas Shift Reaction on Copper. *J. Am. Chem. Soc.* **2008**, *130*, 1402−1414.
(14) Fishtik, I.; Datta, R. A UBI-QEP Microkinetic Model for the Water−Gas Shift Reaction on Cu(111). *Surf. Sci.* **2002**, *512*, 229−254.
(15) Catapan, R. C.; Oliveira, A. A. M.; Chen, Y.; Vlachos, D. G. DFT Study of the Water-Gas Shift Reaction and Coke Formation on Ni(111) and Ni(211) Surfaces. *J. Phys. Chem. C* **2012**, *116*, 20281−20291.
(16) Grabow, L. C.; Gokhale, A. A.; Evans, S. T.; Dumesic, J. A.; Mavrikakis, M. Mechanism of the Water Gas Shift Reaction on Pt: First Principles, Experiments, and Microkinetic Modeling. *J. Phys. Chem. C* **2008**, *112*, 4608−4617.
(17) Chutia, A.; Thetford, A.; Stamatakis, M.; Catlow, C. R. A.; et al. A DFT and KMC Based Study on the Mechanism of the Water Gas Shift Reaction on the Pd(100) Surface. *Phys. Chem. Chem. Phys.* **2020**, *22*, 3620−3632.
(18) Mohsenzadeh, A.; Richards, T.; Bolton, K. DFT Study of the Water Gas Shift Reaction on Ni(111), Ni(100) and Ni(110) Surfaces. *Surf. Sci.* **2016**, *644*, 53−63.
(19) Cao, K.; Fuchsel, G.; Kleyn, A. W.; Juurlink, L. B. F. Hydrogen Adsorption and Desorption from Cu(111) and Cu(211). *Phys. Chem. Chem. Phys.* **2018**, *20*, 22477−22488.
(20) Calle-Vallejo, F.; Loffreda, D.; Koper, M. T.; Sautet, P. Introducing Structural Sensitivity into Adsorption-energy Scaling Relations by Means of Coordination Numbers. *Nat. Chem.* **2015**, *7*, 403−410.
(21) Yang, K.; Zhang, M.; Yu, Y. Theoretical Insights into the Effect of Terrace width and Step Edge Coverage on CO Adsorption and Dissociation over Stepped Ni Surfaces. *Phys. Chem. Chem. Phys.* **2017**, *19*, 17918−17927.
(22) Hammer, B.; Nørskov, J. K. Electronic Factors Determining the Reactivity of Metal Surfaces. *Surf. Sci.* **1995**, *343*, 211−220.
(23) Yang, F. F.; Liu, D.; Wang, H.; Liu, X.; Han, J. Y.; Ge, Q. F.; Zhu, X. L. Geometric and Electronic Effects of Bimetallic Ni-Re Catalysts for Selective Deoxygenation of m-Cresol to Toluene. *J. Catal.* **2017**, *349*, 84−97.
(24) Kresse, G.; Hafner, J. Ab Initio Molecular Dynamics for Liquid Metals. *Phys. Rev. B* **1993**, *47*, 558−561.
(25) Kresse, G.; Hafner, J. Ab Initio Molecular-Dynamics Simulation of the Liquid-Metal Amorphous-Semiconductor Transition in Germanium. *Phys. Rev. B* **1994**, *49*, 14251−14269.
(26) Kresse, G.; Furthmuller, J. Efficiency of Ab-Initio Total Energy Calculations for Metals and Semiconductors Using a Plane-Wave Basis Set. *Comput. Mater. Sci.* **1996**, *6*, 15−50.
(27) Kresse, G.; Furthmuller, J. Efficient Iterative Schemes for Ab Initio Total-Energy Calculations Using a Plane-Wave Basis Set. *Phys. Rev. B* **1996**, *54*, 11169−11186.
(28) Pan, Y.; Zhang, H.; Shi, D.; Sun, J.; Du, S.; Liu, F.; Gao, H. J. Highly Ordered, Millimeter Scale, Continuous, Single-Crystalline Graphene Monolayer Formed on Ru(0001). *Adv. Mater.* **2009**, *21*, 2777−2780.
(29) Blöchl, P. E. Projector Augmented-Wave Method. *Phys. Rev. B* **1994**, *50*, 17953.
(30) Henkelman, G.; Uberuaga, B. P.; Jonsson, H. A Climbing Image Nudged Elastic Band Method for Finding Saddle Points and Minimum Energy Paths. *J. Chem. Phys.* **2000**, *113*, 9901−9904.
(31) Henkelman, G.; Jonsson, H. Improved Tangent Estimate in the Nudged Elastic Band Method for Finding Minimum Energy Paths and Saddle Points. *J. Chem. Phys.* **2000**, *113*, 9978−9985.
(32) Calle-Vallejo, F.; Martinez, J. I.; Garcia-Lastra, J. M.; Sautet, P.; Loffreda, D. Fast Prediction of Adsorption Properties for Platinum Nanocatalysts with Generalized Coordination Numbers. *Angew. Chem., Int. Ed.* **2014**, *53*, 8316−8319.
(33) Xu, S. M.; Yan, H.; Wei, M. Band Structure Engineering of Transition-Metal-Based Layered Double Hydroxides toward Photocatalytic Oxygen Evolution from Water: A Theoretical-Experimental Combination Study. *J. Phys. Chem. C* **2017**, *121*, 2683−2695.
(34) Hammer, B.; Nørskov, J. K. Electronic Factors Determining the Reactivity of Metal Surfaces. *Surf. Sci.* **1995**, *343*, 211−220.
(35) Hammer, B.; Nørskov, J. K. Theoretical Surface Science and Catalysis Calculations and Concepts. *Adv. Catal.* **2000**, *45*, 71−129.
(36) Kozuch, S.; Shaik, S. A Combined Kinetic-Quantum Mechanical Model for Assessment of Catalytic Cycles: Application

to Cross-Coupling and Heck Reactions. *Chem. Commun.* **2011**, *47*, 4935−4937.
(37) Kozuch, S.; Shaik, S. Defining the Optimal Inductive and Steric Requirements for a Cross-Coupling Catalyst Using the Energetic Span Model. *J. Mol. Catal. A: Chem.* **2010**, *324*, 120−126.
(38) Kozuch, S.; Martin, J. M. L. What Makes for a Bad Catalytic Cycle? A Theoretical Study on the Suzuki-Miyaura Reaction within the Energetic Span Model. *ACS Catal.* **2011**, *1*, 246−253.

https://doi.org/10.1021/acsomega.1c05991
ACS Omega 2022, 7, 3514−3521